

Modelling of propagation of very-high-energy γ -rays with CRbeam code. Comparison with CRPropa and ELMAG codes.

O.Kalashev^{1,2}, A.Korochkin^{1,3,4}, A.Neronov^{4,5} and D.Semikoz^{1,4,6}

¹ Institute for Nuclear Research of the Russian Academy of Sciences, 60th October Anniversary st. 7a, 117312, Moscow, Russia

² Moscow Institute for Physics and Technology, 9 Institutskiy per., Dolgoprudny, Moscow Region, 141701 Russia

³ Novosibirsk State University, Pirogova 2, Novosibirsk, 630090 Russia

⁴ Université de Paris, CNRS, Astroparticule et Cosmologie, F-75013 Paris, France

⁵ Astronomy Department, University of Geneva, Ch. d'Ecogia 16, 1290, Versoix, Switzerland

⁶ National Research Nuclear University MEPhI, 115409 Moscow, Russia

January 12, 2022

ABSTRACT

Context. Very-high-energy γ -rays produce electron positron pairs in interactions with low-energy photons of extragalactic background light during propagation through the intergalactic medium. The electron-positron pairs generate secondary γ -rays detectable by γ -ray telescopes. This secondary emission can be used to detect Inter-Galactic Magnetic Fields (IGMF) in the voids of Large Scale Structure. *Aims.* New γ -ray observatory, Cherenkov Telescope Array (CTA), will provide an increase of sensitivity for detection of these secondary γ -ray emission and enable measurement of its properties for sources at cosmological distances. Interpretation of the CTA data including detection of IGMF and study of its properties and origin will require precision modelling of the primary and secondary γ -ray fluxes.

Methods. We assess the precision of the modelling of the secondary γ -ray emission using model calculations with publicly available Monte-Carlo codes CRPropa and ELMAG and compare their predictions with theoretical expectations and with model calculations of a newly developed CRbeam code.

Results. We find that model predictions of different codes differ by up to 50% for low-redshift sources, with discrepancies increasing up to order-of-magnitude level with the increasing source redshifts. We identify the origin of these discrepancies and argue that the new CRbeam code provides reliable predictions for spectral, timing and imaging properties of the secondary γ -ray signal and can be used to study gamma-ray sources and IGMF with precision relevant for the prospective CTA study of the effects of γ -ray propagation through the intergalactic medium.

1. Introduction

The influence of the effect of pair production on the spectra of extragalactic sources of very-high-energy (VHE) γ -rays is nowadays well established via measurements of suppression of the highest energy γ -ray fluxes of blazars (H. E. S. S. Collaboration et al. 2017; Abeyssekara et al. 2019; Acciari et al. 2019). Observations of this effect allow to measure the spectrum of Extragalactic Background Light (EBL) that is difficult to measure directly because of obscuration by Zodiacal light (Matsuura et al. 2017). The EBL is produced by cumulative emission from star forming galaxies accumulated over their cosmological evolution (Franceschini et al. 2008). Its measurement over a range of redshifts provides information on the history of star formation in the Universe (Fermi-LAT Collaboration et al. 2018). γ -ray measurements of EBL are also potentially interesting for the search of narrow features in the EBL spectrum (Korochkin et al. 2020b), such as those produced by axion-like particles (Korochkin et al. 2020a).

Absorption of the VHE γ -rays on EBL results in production of electron-positron pairs in the intergalactic medium. These pairs lose energy on inverse Compton scattering of Cosmic Microwave Background (CMB) photons thus producing secondary γ -ray emission detectable by γ -ray telescopes (Aharonian et al. 1994). Observational appearance of this secondary emission depends on the strength and correlation length of magnetic field in the intergalactic medium and on the energy range of the secondary γ -rays. Very strong intergalactic magnetic field (IGMF)

completely isotropises trajectories of electrons and positrons so that the secondary emission appears as a γ -ray "halo" around primary point source (Aharonian et al. 1994). Moderately strong IGMF induces extended secondary γ -ray emission whose properties depend on the IGMF parameters (Neronov & Semikoz 2007; Murase et al. 2008; Neronov & Semikoz 2009). Weak magnetic field results in the secondary flux morphologically indistinguishable from the point source, but identifiable through specific timing properties (Plaga 1995). Non-detection of the secondary emission in the 1-100 GeV range has been used to derive a lower bound on IGMF at the level of $\sim 10^{-16}$ G under assumption of large IGMF correlation length (Neronov & Vovk 2010; Ackermann et al. 2018).

Sensitivity of observations of the extended or delayed secondary emission from the electron-positron pairs in the intergalactic medium and of the measurements of IGMF will be crucially improved by the Cherenkov Telescope Array (CTA) (Cherenkov Telescope Array Consortium et al. 2019). This will enable search for the extended secondary emission in previously inaccessible energy range thus extending the range of IGMF strengths that can be probed by the γ -ray technique (Korochkin et al. 2021). The sensitivity improvement will result in more precise characterization of the effect of absorption of the primary γ -ray flux by the EBL and more precise measurements of the primary γ -ray source spectra as well as in extension of the measurements into larger redshift range (Abdalla et al. 2021). γ -ray measurements can distinguish primordial magnetic fields pro-

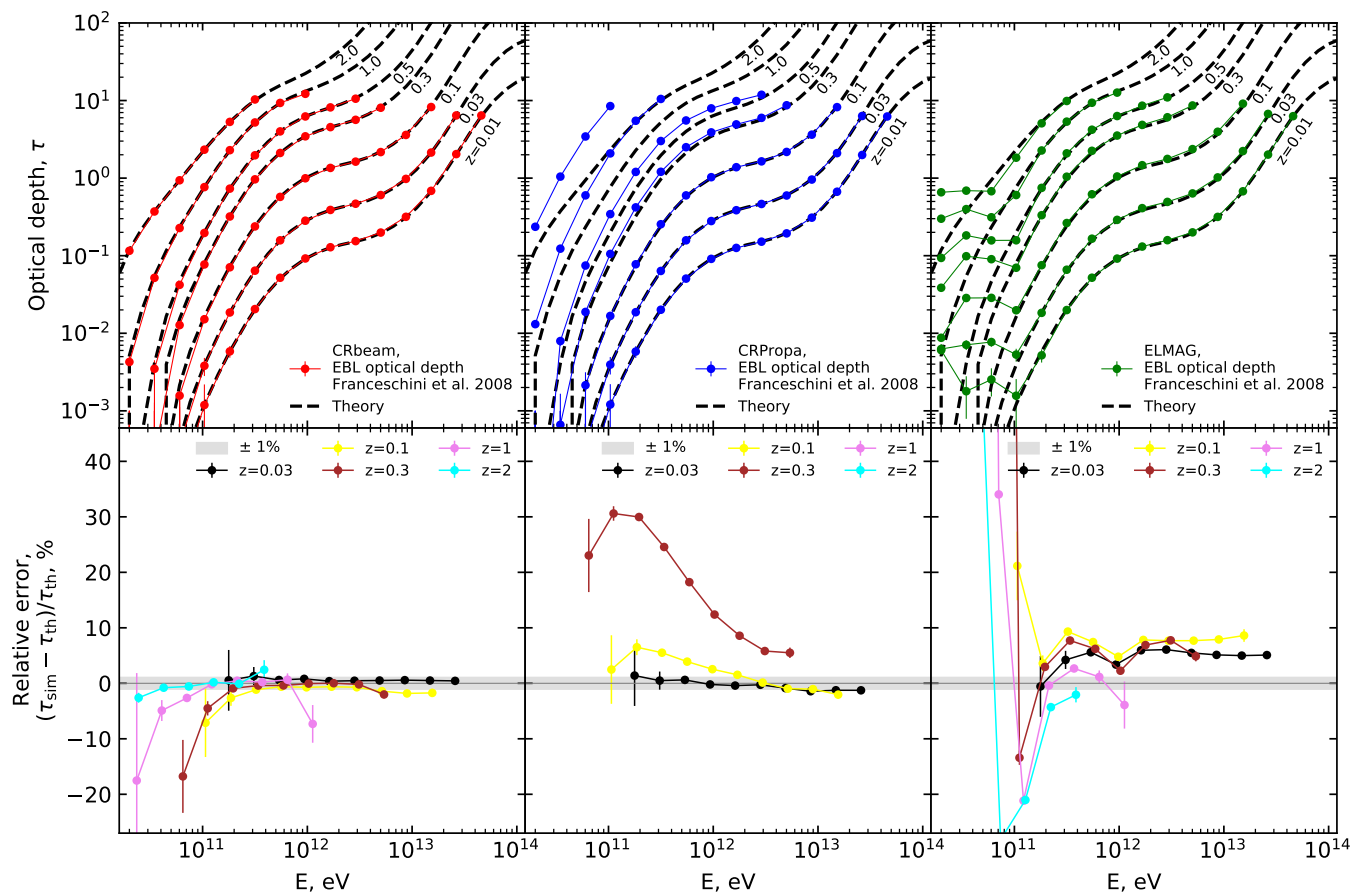


Fig. 1. Comparison of the optical depth for primary γ -rays for sources at cosmological redshifts in CRbeam, CRPropa and ELMAG. In all cases Franceschini et al. (2008) EBL model is assumed. Top panels show the optical depth as a function of γ -ray energy for a range of redshifts. Bottom panels show discrepancies between the code calculations and the analytical model. For CRPropa, the differences between the analytical model and code calculations are not shown for redshifts > 0.3 , because they exceed 50%.

duced during inflation from the field originating from cosmological phase transitions, by constraining the correlation length of the field (Korochkin et al. 2021). Additionally the γ -ray technique is also sensitive to the effect of the baryonic feedback on the Large Scale Structure that creates magnetised bubbles around galaxies (Bondarenko et al. 2021).

Improved sensitivity for the secondary γ -ray flux from extragalactic sources provided by CTA has to be matched by the improved precision of modeling of this flux. Several numerical codes have been previously developed for such modeling, including CRPropa (Alves Batista et al. 2016) and ELMAG (Blytt et al. 2020). These codes are based on Monte-Carlo modeling of development of electromagnetic cascades in the intergalactic medium in the presence of magnetic fields (Elyiv et al. 2009). Details of implementation (of magnetic field structure, of cosmological evolution) differ between the codes. This may lead to code-dependent discrepancies in model predictions of the properties of secondary emission. Each code adopts certain models of the relevant physical processes and Monte-Carlo event generators. This results in systematic modeling errors that are difficult to assess.

In what follows we compare precision of the predictions of the CRPropa and ELMAG with those of the newly developed CRbeam code¹ (first version of the code has been reported by

¹ CRbeam code is available at the link <https://github.com/okolo/mcray/tree/main/src/app/crbeam>

Berezinsky & Kalashev (2016)). The modular structure of the CRbeam and CRPropa allows all relevant processes to be tested independently of each other. Namely, we consider the Breit-Wheeler pair production and inverse Compton scattering on the EBL and CMB. For each interaction, we compare interaction rate and energy distribution of secondary particles inferred from simulations with the theoretical predictions. Also, disabling all interactions makes it possible to compare the propagation of electrons in a magnetic field. For ELMAG, on the contrary, such independent testing of interactions is impossible, therefore we use the results of simulations with ELMAG to compare the properties of the cascade signal, when all relevant interactions are turned on.

We find that the predictions for the spectral, imaging and timing properties of the secondary emission may differ by about 50% in the energy range of interest of CTA. We trace the origin of some of these discrepancies and find that they can be reduced after corrections. We find that differences in implementation of cosmological evolution in CRPropa and CRbeam still lead to non-negligible differences between model calculation in the two frameworks for sources at large redshifts, because of the known limitation of the CRPropa.

In all further analysis, we used the following versions of the codes: CRbeam 1.0, CRPropa3-3.1.7 and ELMAG 3.01. Additionally, we have verified that the results of CRPropa are stable

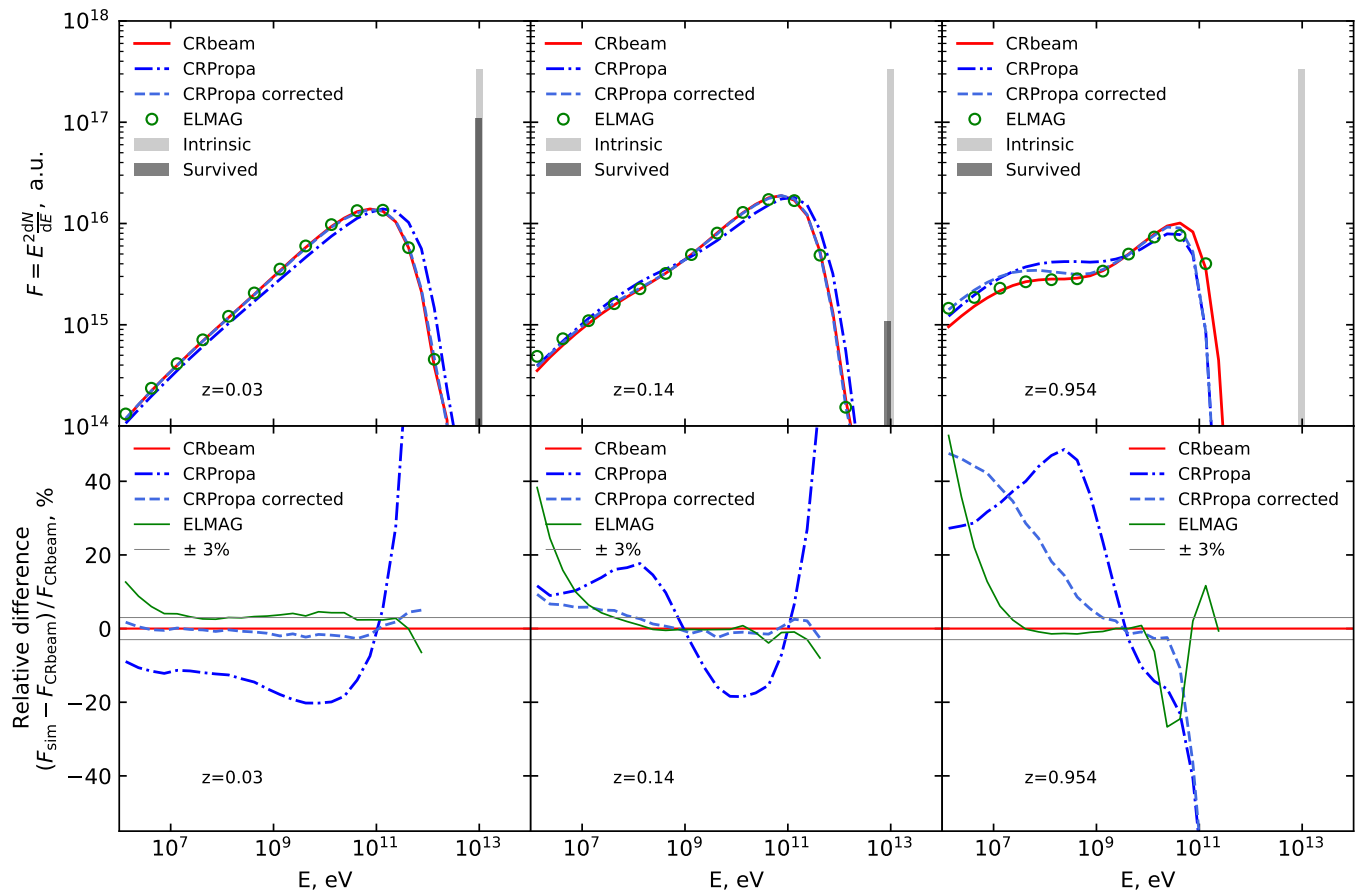


Fig. 2. Differences in model predictions for the spectra of secondary γ -rays produced by interaction of monoenergetic primary γ -ray beam with energy $E_{\gamma_0} = 10$ TeV. Top panels shows the primary and secondary γ -ray spectra for sources at different redshifts. Bottom panels show the differences between CRbeam, CRPropa and ELMAG models.

in relation to previous versions CRPropa3-3.1.5 and CRPropa3-3.1.6.

2. Absorption of the primary γ -rays

We start our comparison from the modeling of absorption of primary γ -rays on EBL. Fig. 1 shows comparison of the calculated optical depths for photons of different energies. All calculations are done for the Franceschini et al. (2008) EBL model. One can see that CRbeam modeling reproduces the assumed analytical model with percent-level precision in the energy range above 200 GeV for a wide range of source redshifts. Differences up to 20% at the energies $E < 100$ GeV do not have large effects on the model results because the optical depth in this energy range is small even for sources at redshift $z \sim 1$.

The results of simulations with ELMAG are also in good agreement with theory in the energy region above 100 GeV, although it predicts $\sim 5\%$ larger optical depth. Strong differences from theory are clearly noticeable in the energy range 10-100 GeV, where ELMAG predicts a significantly higher optical depth. For sources with redshifts $z \lesssim 0.5$, this discrepancy will have no effect, since in this case even the wrong optical depth is much less than unity. Nevertheless, differences may arise for sources with $z \sim 1$, since in this case in the ELMAG the optical depth $\tau \sim 1$, and not less than unity as it should be according to the theory.

To the contrary, the calculations of CRPropa differ significantly from the assumed analytical model already for sources at redshifts $z \gtrsim 0.3$. The difference reaches 30% at 100 GeV for the source at redshift $z = 0.3$ and reaches up to 100% for further away sources (not shown in the bottom panel of the figure). The discrepancy between the numerical and analytical model in the CRPropa code are due to simplified evolution of the EBL with redshift in which the real evolution of EBL is replaced by the renormalization of EBL spectrum taken at $z = 0$ with a factor $s(z)$ (Alves Batista et al. 2016). This CRPropa limitation is known (Alves Batista et al. 2016). Our result shows explicitly that such a simplification starts to produce incorrect results already starting from moderate redshifts ~ 0.3 .

3. Emission of secondary γ -rays via inverse Compton scattering

Precision of the modeling of properties of the secondary γ -ray emission depends on the precision of calculation of the optical depth of the primary γ -ray flux (discussed in the previous section), of the energy distribution of the produced pairs and of the differential cross-section of inverse Compton scattering.

An example calculation of secondary γ -ray spectrum by CRbeam is shown in Fig. 2 for a monoenergetic primary γ -ray source at different redshifts corresponding to known blazar type active galactic nuclei Mrk 421 ($z = 0.03$), 1ES 0229+200

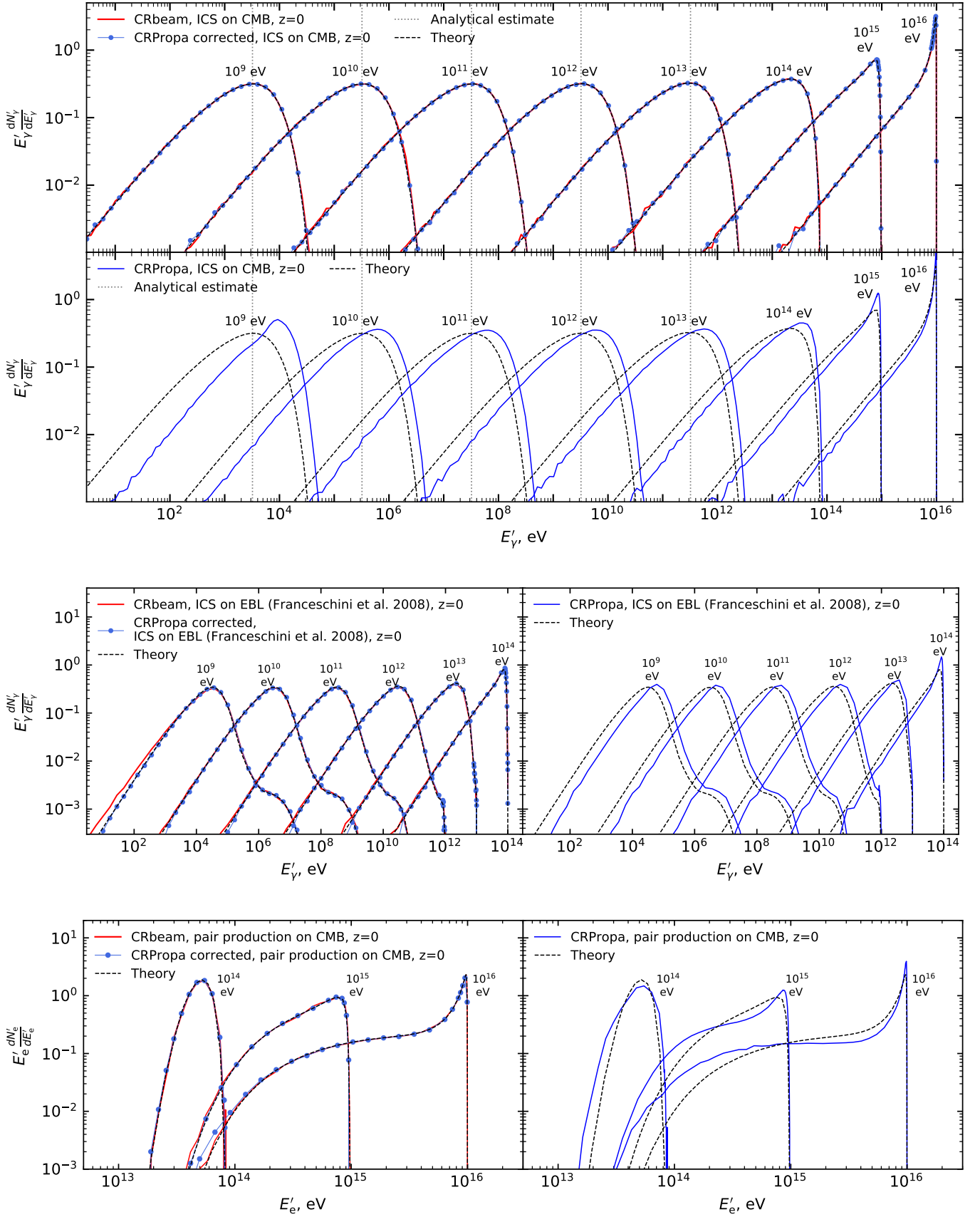


Fig. 3. Top: energy distribution of γ -rays produced via ICS on CMB by electrons with different energies (indicated as tags for each set of spectra). Middle: spectra of γ -rays from ICS on EBL for a range of electron energies. Bottom: Energy spectra of pairs produced in interactions of γ -rays with CMB photons. Energies of the primary γ -rays are shown as tags for each group of spectra. In all cases the codes used for the model calculations are specified in the legend.

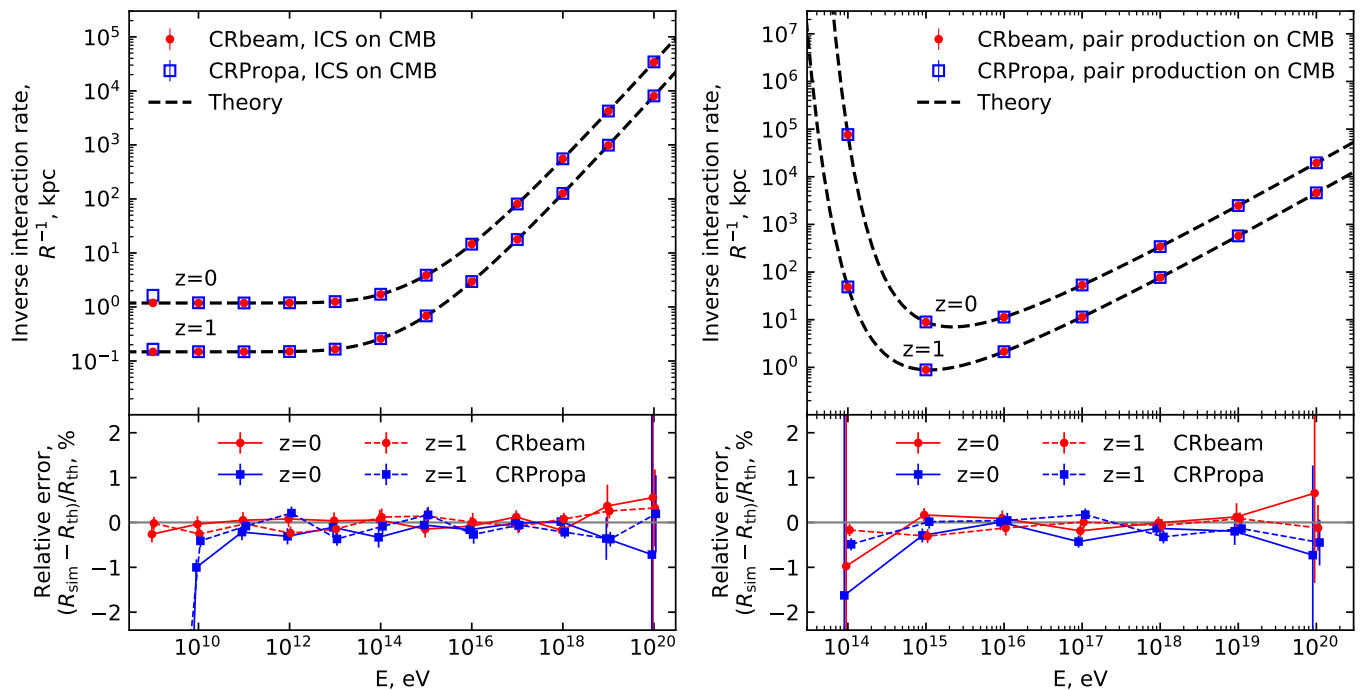


Fig. 4. Interaction rates for the pair production and inverse Compton scattering on the CMB at the redshifts $z = 0$ and $z = 1$.

($z = 0.14$) and PKS 0502+049 ($z = 0.954$), covering a wide range of redshifts.

We find significant discrepancies that reach 50% for CRbeam-CRPropa comparison and some 30% for CRbeam-ELMAG, in the case of the source at the redshift $z \sim 1$. Smaller discrepancies, at the level of 20% over a broad energy range up to 100 GeV are found for smaller redshift sources. Nevertheless, also in this case the discrepancies rise to $> 50\%$ at the high energy end of the secondary γ -ray spectrum.

The difference in cascade signal between CRbeam and ELMAG can be fully explained by the difference in the optical depth for the primary γ -rays. Indeed, for a nearby source with a redshift $z = 0.03$, a 5% greater optical depth for 10 TeV gamma rays results in a 5% amplification of the cascade signal over the entire energy range. For a more distant source with $z = 0.14$, most of the primary gamma rays are absorbed; therefore, a 5% difference in the optical depth does not appear and the normalization of the cascade signals in the region above 100 MeV coincide. However, increased absorption leads to an increase in the suppression of the high-energy part of the secondary signal. This is manifested in the fact that in the ELMAG the cascade signal is weaker in the region above 100 GeV and stronger in the region below 100 MeV. The same is true for a source at the redshift $z = 0.954$. In addition, a dip at 10-100 GeV noticeable in the ELMAG spectrum corresponds to the order-of-magnitude excess absorption in ELMAG in this energy range, which leads to an even stronger amplified cascade signal below 100 MeV.

Unlike ELMAG, the difference between CRPropa and CRbeam cannot be explained by this single cause. Part of the discrepancy is certainly due to the differences in the calculation of the optical depth for the primary γ -rays producing pairs on the EBL. However, further differences in the modeling of the secondary flux are involved. This is indicated by the significant differences of the results of calculation with different codes for low-redshift sources, for which the optical depth calculations do not show strong discrepancies.

We have found that for the low-redshift sources the main difference comes from the calculation of the inverse Compton scattering spectra by electrons and positrons. Figure 3 shows a comparison of analytically calculated spectra of the inverse Compton scattering on the CMB with the output of CRbeam and CRPropa for this process. One can see that the CRPropa calculations do not match the theoretical formula. The discrepancies are of the order-of-one all over the energy range of the inverse Compton emission for electrons with energies up to 10^{16} eV. This large discrepancy is "smeared" and becomes less noticeable in the calculation of the spectrum of inverse Compton emission from a broad energy distribution of electrons shown in Fig. 2.

We have also identified a similar problem of the CRPropa code in calculation of the inverse Compton scattering (ICS) on the EBL (see middle panel of Fig. 3) and in the spectra of $\gamma\gamma$ pair production. Bottom panel of Fig. 3 illustrates this problem for the case of pair production on CMB. In CRPropa, the electron-positron spectrum differs from the known analytical formulae (Gould & Schröder 1967), shown by the dashed lines.

Having noticed these discrepancies, we analyzed the implementation of the CRPropa code and found out that the error with the energy distribution of secondary particles has a common origin for all three cases (ICS on CMB, ICS on EBL and pair-production on CMB). The error occurs from the pre-calculated tables that come with the code. These tables are used to sample the energy at the center of mass as the interaction occurs. After recalculating the tables, the results obtained with the CRPropa with these corrected tables match analytical calculations, as can be seen from Fig. 3 (in all plots, we use the 'CRPropa corrected' label for the CRPropa with recalculated tables). After this correction, model calculations of the spectra of secondary emission for our benchmark case of monoenergetic primary γ -ray beam agree between CRbeam and CRPropa for low-redshift sources down to $\leq 5\%$ level, see Fig. 2. The discrepancies still grow with increasing source redshift, for the reasons explained in the previous section.

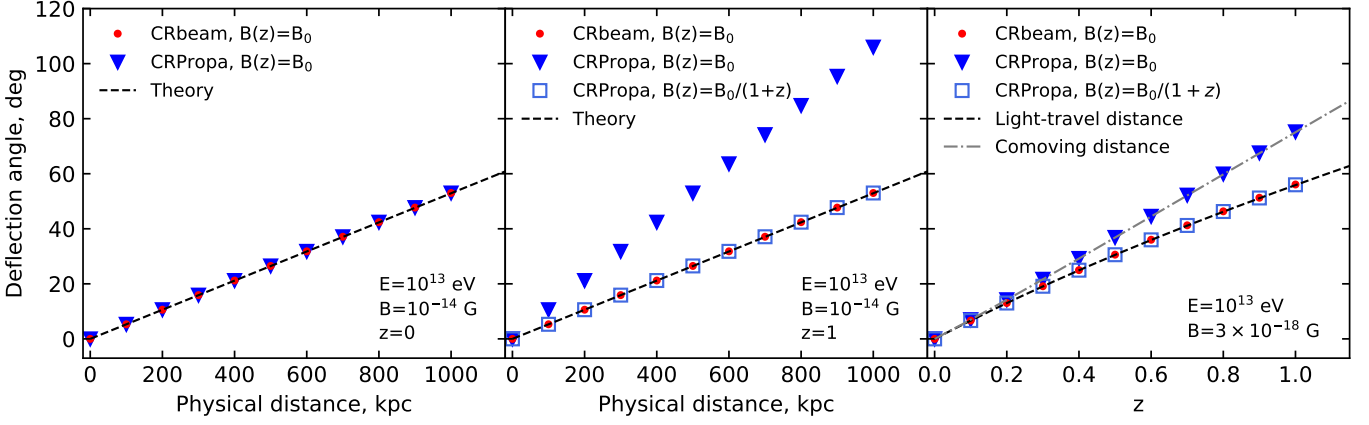


Fig. 5. Deflection of electrons of different energies in constant magnetic field with fixed physical strength in CRbeam and CRPropa.

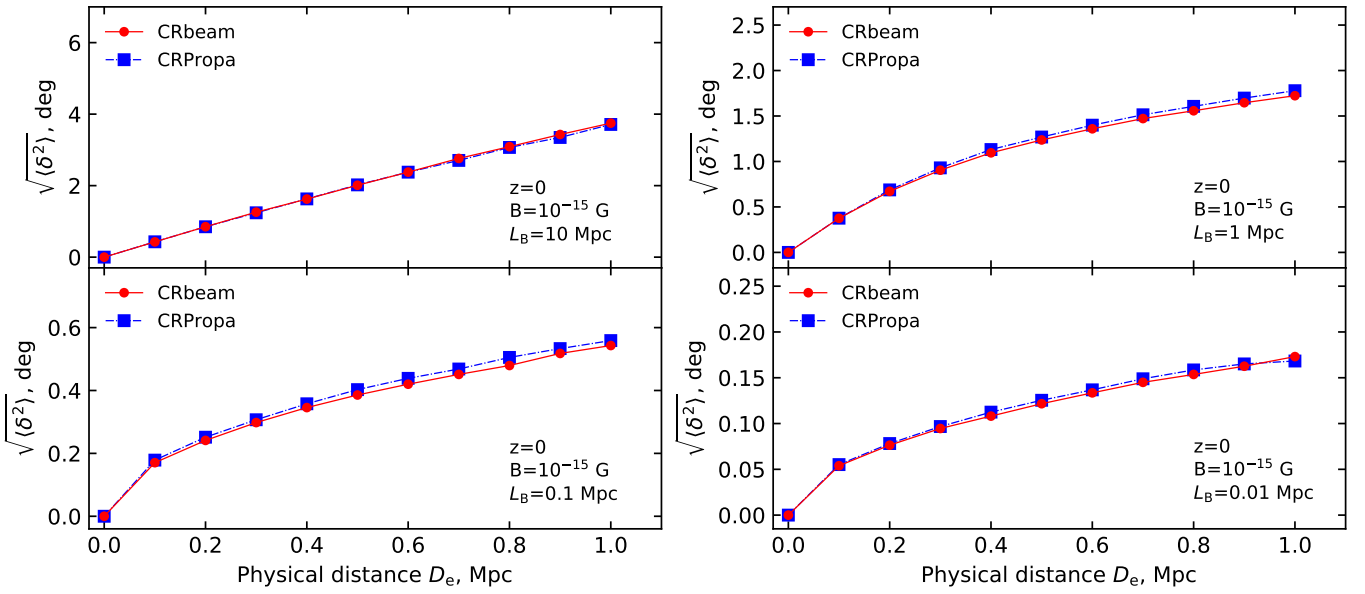


Fig. 6. Deflections of electrons in turbulent magnetic fields with different correlation lengths. Left panels show the root mean square deflection angle dependence on the physical path length, right panels show the distribution of deflection angles after certain path lengths.

We have also verified that the interaction rates for inverse Compton scattering and pair production on CMB calculated using CRbeam and CRPropa are in agreement with each other and with a relative difference from theory not exceeding one percent, see Fig.4. 30% less ICS interaction rate in CRPropa for energies less than 10 GeV is present only in the version CRPropa3-3.1.7 and absent in previous versions.

4. Propagation of electrons and positrons

Imaging and timing properties of the secondary γ -ray signal are determined by the details of propagation of electrons and positrons under the influence of IGMF. The inverse Compton scattered γ -rays are emitted after electrons and positrons are deflected by an angle δ determined by the energy of electron E_e and strength of the magnetic field B . In the simplest case of homogeneous magnetic field the angle is given by the analytical formula

$$\delta = \frac{D}{R_L} = \frac{eB}{E_e} D \quad (1)$$

where e is the electron charge, D is the propagation distance and $R_L = E_e/eB$ is the gyroradius.

Both CRPropa and CRbeam correctly solve equations of motions of the electrons in magnetic fields. However, the approaches of the two codes differ when accounting for cosmological effects. In CRbeam, the particle coordinates are expressed in physical distances, while in CRPropa, the comoving coordinates are used. This difference can be illustrated by a simple test where the electron is deflected by a homogeneous magnetic field that is perpendicular to the electron's velocity. Figure 5 shows the calculation of deflection angle of electrons for this simplest case, found with CRbeam and CRPropa codes. One can see that both calculations give the same result at the redshift $z = 0$ where physical and comoving distance elements are equal, left panel of Fig.5. However, the CRPropa calculation predicts $(1+z)$ stronger deflection at the redshift $z = 1$, which is explained by the fact that $dx_{\text{comoving}} = (1+z)dx_{\text{physical}}$, so that electron travels $(1+z)$ longer distance in the same magnetic field, see middle panel of Fig.5.

This difference becomes most pronounced when the electron travels over cosmological distances. Right panel of Fig. 5 shows the deflection of electron starting at redshift z (x-axis of the panel) and caught at $z = 0$. One can see that the deflection angles in CRPropa are proportional to the comoving distances and in CRbeam to the light travel distances. The simplest way to get the correct deflection angles in CRPropa is to set the evolution of the magnetic field with redshift, namely $B(z) = B_0/(1+z)$, what can be done using the built-in methods of CRPropa.

The field re-scaling trick can also be used when an electron propagates in a realistic turbulent magnetic field if the correlation length of this field is greater than the electron propagation length. Nevertheless, it is not clear how to construct the correct trajectories when the correlation length of the magnetic field is comparable to or less than the propagation length of an electron. We have compared the results on electron deflection also for this case. For the magnetic field we used Kolmogorov spectrum with the maximum scale L_B and minimum scale equal to $L_B/100$. Fig. 6 shows the dependence of deflection angle on propagation distance for electrons moving in turbulent magnetic fields. The codes are in good agreement with each other and reproduce analytical formula of (Neronov & Semikoz 2009) in case of small correlation length

$$\sqrt{\langle \delta^2 \rangle} = \sqrt{\frac{D\lambda_B}{R_L}} = \sqrt{\frac{D\lambda_B e B}{E_e}} \quad (2)$$

where λ_B is the magnetic field correlation length. For the Kolmogorov spectrum $\lambda_B \approx L_B/5$.

We also tested the turbulent magnetic field generator in ELMAG. Using the built-in `test_turbB` function, we separately calculated the average value of each component of the magnetic field. Assuming that the field of the strength B is uniform and isotropic, it was expected that

$$\sqrt{\langle B_x^2 \rangle} = \sqrt{\langle B_y^2 \rangle} = \sqrt{\langle B_z^2 \rangle} = B/\sqrt{3} \quad (3)$$

As a result of tests, we found that the values of the x and y components of the magnetic field are about 20 percent less than predicted theoretically, while there is no such difference for the z component. The reason for this was not found, so we simply re-scaled the x and y components of the field to the correct value. The results of ELMAG with such a re-scaled field are indicated on the plots as 'ELMAG corrected'.

5. Properties of primary and secondary emission from sources at different distances

Realistic modeling of spectral, imaging and timing properties of the primary and secondary γ -ray signals from extragalactic sources combines the modeling of the pair production, inverse Compton scattering and electron propagation discussed above. Discrepancies in the modeling of these ingredients propagate to the discrepancies of the overall signal models. We discuss these discrepancies in this section.

Left side of Fig. 7 shows the result of modeling of the primary and secondary γ -ray signals for the nearby blazars like Mrk 421 and Mrk 501. As discussed in Section 2, all the codes provide identical predictions for the optical depth for the primary γ -rays in this case. As noticed in Section 3, predictions for the spectra of pair production and inverse Compton scattering in the CRPropa code deviate from known analytical formulae. This leads to discrepancies between the models of secondary γ -ray

fluxes in CRbeam and CRPropa codes, noticeable in the TeV energy range, which is most interesting for CTA. Top panel of the figure shows that the differences reach a factor-of-two above 3 TeV. Middle and bottom panels of the figure show the temporal and angular profiles of extended emission. The differences in the spectral properties of the secondary signal between CRbeam and CRPropa are not so pronounced in the low-energy temporal and angular profiles in the lower energy bands, accessible to Fermi/LAT telescope. However, these differences grow in the CTA energy band above 100 GeV. As discussed in Section 3, the discrepancy between the CRbeam and CRPropa predictions can be removed after a correction to the CRPropa code. In this case, all the codes produce results that agree at $\sim 10\%$ level, as can be seen from the left side of Fig. 7.

To the contrary, corrections to the CRPropa code do not remove the discrepancies between different model predictions for a source at large redshift, see right side of Fig. 7. Very significant difference in model predictions is noticeable at the highest energy ends of the spectra, visible in the top right panel of Fig. 7. CRPropa predicts strong suppression of the flux above 200 GeV, while CRbeam predicts a gradual suppression in the energy range between 200 and 300 GeV. This discrepancy is crucially important for the study of high-redshift sources with CTA. Such modeling errors reaching order-of-magnitude have to be removed before any sensible results on the EBL evolution can be extracted from the CTA data. The discrepancy is noticeable also in the attenuated primary source spectra shown by the grey curves in Fig. 7. We attribute this discrepancy to the incorrect modeling of absorption on EBL for high redshift sources in CRPropa, as described in Section 2.

Similarly large are discrepancies in the timing and imaging properties of the secondary γ -ray signal, shown in the middle and bottom panels on the right side of Fig. 7. Contrary to the low-redshift sources, differences in predictions for the peaking time of the delayed signal are large already for lower energy γ -rays detectable with Fermi/LAT.

The results for the source 1ES 0229+200 at redshift $z = 0.14$ are presented in Fig. 8. Calculations are done for IGMF with Kolmogorov spectrum with strength $B = 10^{-15}$ G and maximum scale $L_B = 10$ Mpc. In this figure the full cascade contribution for zero magnetic field is denoted as 'full'. The curves marked 'jet' show the extended and delayed fluxes for non-zero IGMF for different angular and time intervals. The results for the CRbeam code are compared with CRPropa and ELMAG before (upper panel) and after (lower panel) corrections. All codes give similar results for most of the parameters, after corrections.

6. Discussion

Our comparative study of model predictions for the primary and secondary very-high-energy γ -ray signals from astronomical sources at different redshifts has revealed significant differences in model predictions obtained with different Monte-Carlo codes CRbeam, CRPropa and ELMAG. Most remarkably, we have identified large differences in model calculations of observables crucial for cosmological probes that will be enabled by the new CTA γ -ray observatory.

The largest discrepancies, which reach up to order-of-magnitude, are found for the sources at high redshift of the order of $z = 1$. In this case, CRPropa code predicts a sharp suppression of both primary and secondary signals between 100 GeV and 200 GeV, with no flux detectable above 200 GeV. To the contrary, calculations with CRbeam code show that the flux is suppressed only above 300 GeV.

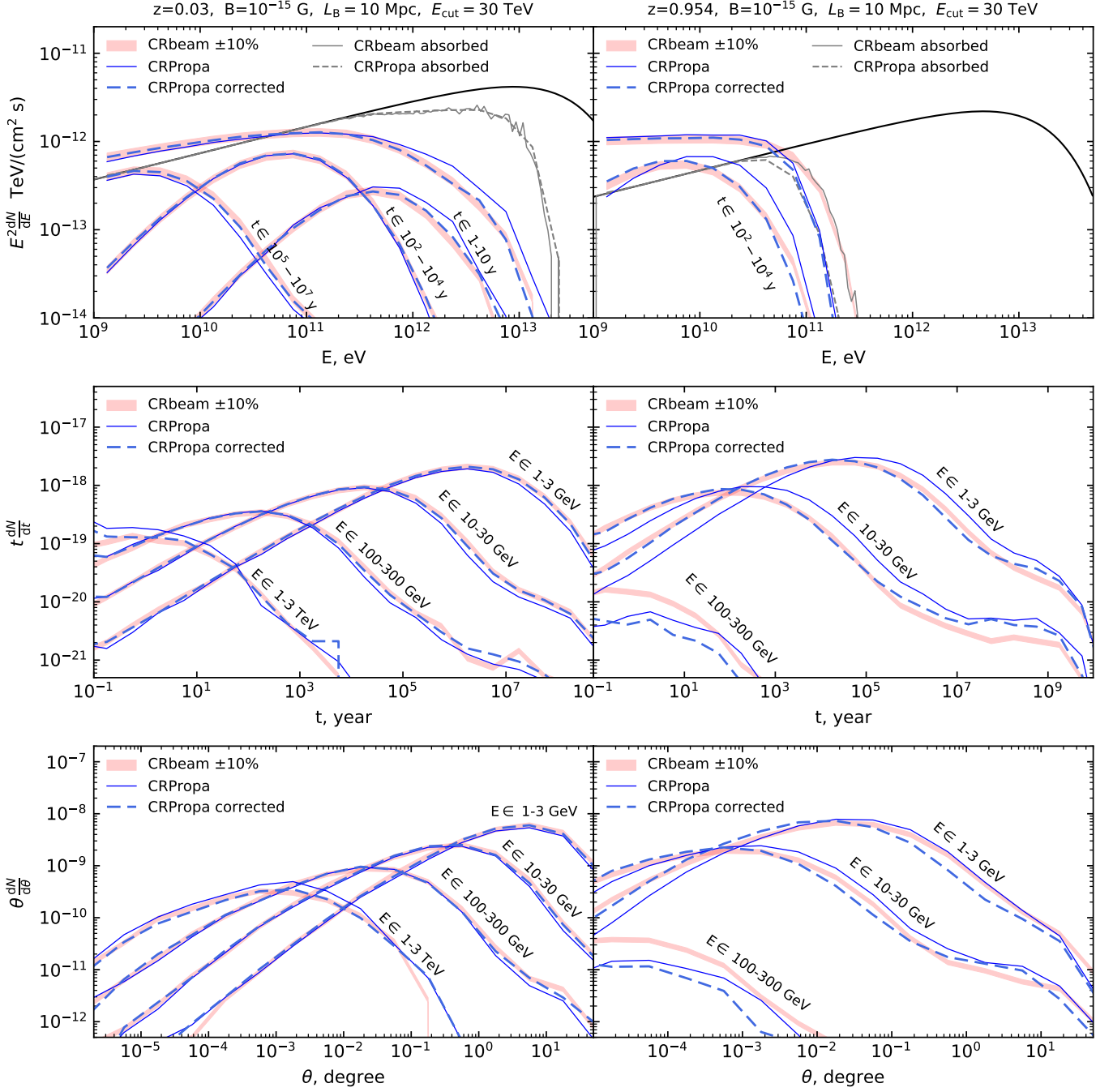


Fig. 7. Spectral (top), timing (middle) and imaging (bottom) properties of primary and secondary γ -ray signals for a IGMF with strength 10^{-15} G and 10 Mpc correlation length. Left panels show calculations for the source at redshift $z = 0.03$, right panels are for the source at redshift $z = 0.954$. Calculations with CRbeam code (red solid) compared with CRPropa (blue thin solid) and corrected CRPropa (blue dashed) codes.

Discrepancies in model predictions would hamper the possibility of doing cosmology with CTA, unless they are understood and removed. We have identified the origin of most of these discrepancies, notably in the modeling of attenuation of γ -rays and deflections of electrons in the CRPropa code. Once corrections are introduced to the CRPropa code, the discrepancies are reduced to $\sim 10\%$. This number can be considered as an estimate of the systematic modeling error in the measurements of cosmological evolution of EBL and measurements of IGMF with CTA.

Acknowledgements. Work of A.K. was supported in part by Russian Science Foundation grant 20-42-09010. A.K.'s stay in the APC laboratory was provided by the ‘‘Vernadsky’’ scholarship of the French embassy in Russia. The work of D.S. and A.N. has been supported in part by the French National Research Agency (ANR) grant ANR-19-CE31-0020.

References

- Abdalla, H. et al. 2021, JCAP, 02, 048
 Abeysekara, A. U., Archer, A., Benbow, W., et al. 2019, ApJ, 885, 150
 Acciari, V. A., Ansoldi, S., Antonelli, L. A., et al. 2019, MNRAS, 486, 4233

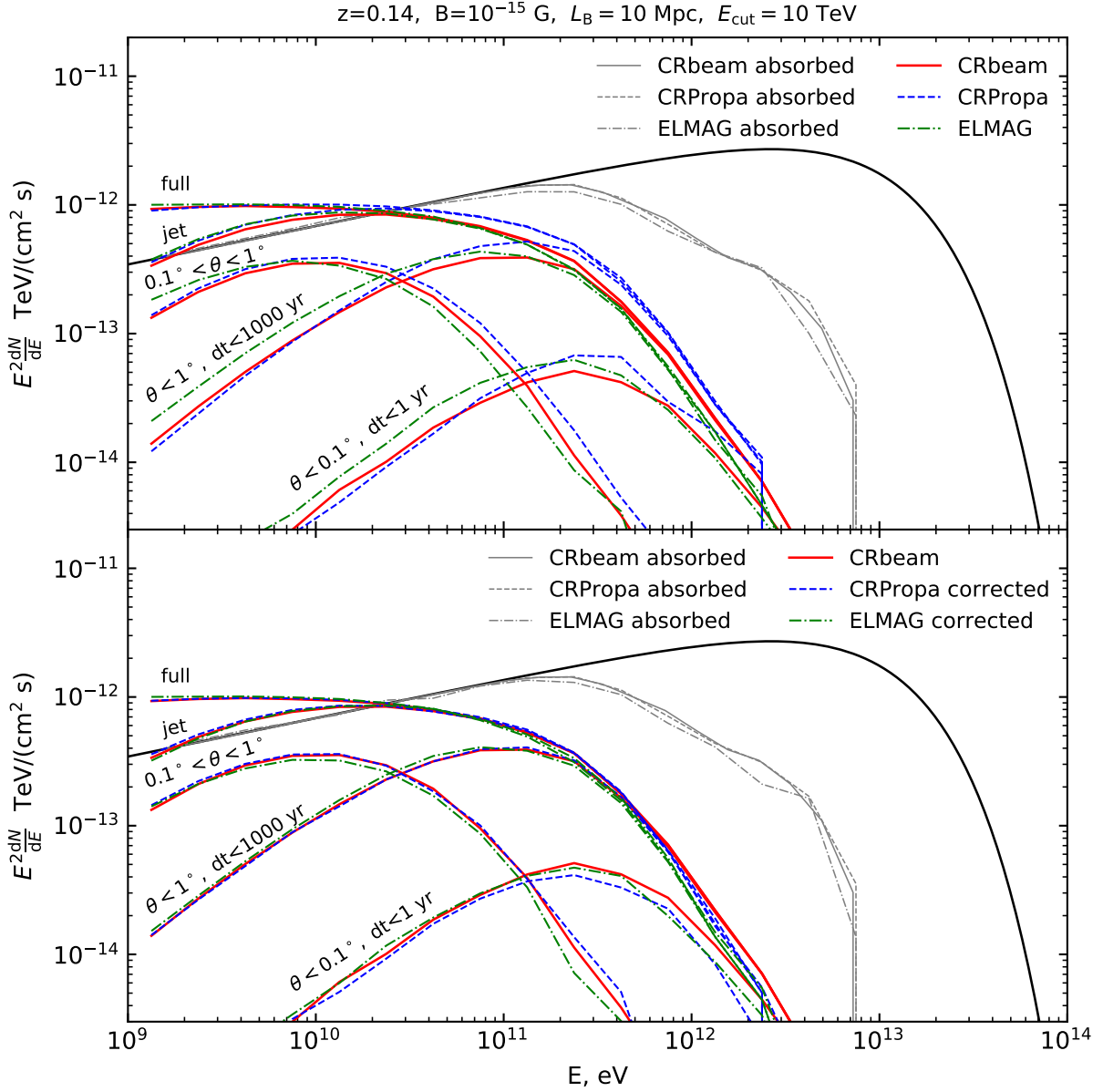


Fig. 8. Cascade contributions for the source at the redshift $z = 0.14$ and for a turbulent IGMF with Kolmogorov spectrum with strength $B = 10^{-15} \text{ G}$ and maximum scale $L_B = 10 \text{ Mpc}$ (corresponding correlation length $\lambda_B \approx 2 \text{ Mpc}$). The jet opening angle was assumed to be $\theta_{\text{jet}} = 5^\circ$, and the observer was at an angle $\theta_{\text{obs}} = 3^\circ$ with respect to the jet axis. Red solid lines is for CRbeam code, blue dashed lines is for CRPropa code and green dash-dotted lines - ELMAG code. Line labels indicate the constraints on the source activity time dt and angular distance from the source θ that were used when constructing the cascade signal. Label 'jet' denotes the cascade signal without constraints on dt ($dt = \infty$) and θ ($\theta = 2\pi$). For comparison, we also added a cascade spectrum in the absence of a magnetic field (label 'full').

Ackermann, M., Ajello, M., Baldini, L., et al. 2018, *The Astrophysical Journal Supplement Series*, 237, 32
 Aharonian, F. A., Coppi, P. S., & Voelk, H. J. 1994, *ApJ*, 423, L5
 Alves Batista, R., Dundovic, A., Erdmann, M., et al. 2016, *J. Cosmology Astropart. Phys.*, 2016, 038
 Berezhinsky, V. & Kalashev, O. 2016, *Phys. Rev. D*, 94, 023007
 Blytt, M., Kachelrieß, M., & Ostapchenko, S. 2020, *Computer Physics Communications*, 252, 107163
 Bondarenko, K., Boyarsky, A., Korochkin, A., et al. 2021 [arXiv:2106.02690]
 Cherenkov Telescope Array Consortium, Acharya, B. S., Agudo, I., et al. 2019, *Science with the Cherenkov Telescope Array*
 Elyiv, A., Neronov, A., & Semikoz, D. V. 2009, *Phys. Rev. D*, 80, 023010
 Fermi-LAT Collaboration, Abdollahi, S., Ackermann, M., et al. 2018, *Science*, 362, 1031
 Franceschini, A., Rodighiero, G., & Vaccari, M. 2008, *A&A*, 487, 837
 Gould, R. J. & Schröder, G. P. 1967, *Phys. Rev.*, 155, 1404

H. E. S. S. Collaboration, Abdalla, H., Abramowski, A., et al. 2017, *A&A*, 606, A59
 Korochkin, A., Kalashev, O., Neronov, A., & Semikoz, D. 2021, *ApJ*, 906, 116
 Korochkin, A., Neronov, A., Lavaux, G., Ramsøy, M., & Semikoz, D. 2021 [arXiv:2111.10311]
 Korochkin, A., Neronov, A., & Semikoz, D. 2020a, *JCAP*, 03, 064
 Korochkin, A., Neronov, A., & Semikoz, D. 2020b, *Astron. Astrophys.*, 633, A74
 Matsuura, S., Arai, T., Bock, J. J., et al. 2017, *ApJ*, 839, 7
 Murase, K., Takahashi, K., Inoue, S., Ichiki, K., & Nagataki, S. 2008, *Astrophys. J. Lett.*, 686, L67
 Neronov, A. & Semikoz, D. V. 2007, *JETP Lett.*, 85, 589
 Neronov, A. & Semikoz, D. V. 2009, *Phys. Rev. D*, 80, 123012
 Neronov, A. & Vovk, I. 2010, *Science*, 328, 73
 Plaga, R. 1995, *Nature*, 374, 430